Evidence for nonmigrating thermal tides in the Mars upper atmosphere from the Mars Global Surveyor Accelerometer Experiment

R. John Wilson

Geophysical Fluid Dynamics Laboratory/NOAA, Princeton University, Princeton, New Jersey, USA

Received 23 August 2001; accepted 14 November 2001; published 11 April 2002.

[1] Mars Global Surveyor Accelerometer Experiment density measurements indicate the presence of planetary-scale wave structure in the Mars upper atmosphere (~130 km). In particular, Phase 2 aerobraking observations reveal large amplitude zonal wave 2 and 3 variations in dayside density between ± 60° latitude. These spatial variations (in a fixed local solar time reference) can be qualitatively reproduced by a Mars general circulation model and are identified as a manifestation of eastward propagating nonmigrating thermal tides with long vertical wavelengths. The simulated wave 2 variation is dominated by a diurnal period wave 1 Kelvin mode while the principal components of the simulated zonal wave 3 structure are a diurnal period wave 2 Kelvin mode and a wave 1 semidiurnal tide. The characterization of these waves is important for understanding the structure and variability of the martian atmosphere at aerobraking altitudes. *INDEX TERMS:* 5409 Planetology: Solid Surface Planets: Atmospheres—structure and dynamics; 5445 Planetology: Solid Surface Planets: Meteorology (3346); 3384 Meteorology and Atmospheric Dynamics: Waves and tides

1. Introduction

[2] The Mars Global Surveyor (MGS) Accelerometer Experiment (ACC) has provided an extensive set of density profiles of the Mars upper atmosphere at altitudes from 110 to 160 km for two distinct seasons [*Keating et al.*, 1998; *Withers et al.*, 2000; *Keating et al.*, 2001]. Densities at 125 km derived from dayside Phase 1 aerobraking measurements between 30° and 50°N indicate the presence of large amplitude longitudinal variations during the Northern Hemisphere (NH) fall / winter season [*Keating et al.*, 1998]. These variations have a prominent zonal wave 2 component which was interpreted as resulting from the propagation of a topographically forced, stationary Rossby wave into the thermosphere [*Keating et al.*, 1998]. Phase 2 aerobraking observations obtained during the NH spring season have also revealed large amplitude longitudinal variability in dayside density at 130 km, with planetary-scale structure extending from 60°N to 80°S [*Withers et al.*, 2000]. *Withers et al.* [2000] showed that there were significant differences in the longitudinal structure of dayside and nightside density between 30°S and 80°S and argued that the stationary wave model was inconsistent with the evident dependence on local solar time (LT). This finding supports recent suggestions that thermal tides should be prominent in the thermosphere [*Joshi et al.*, 2000; *Forbes and Hagan*, 2000; *Wilson*, 2000].

[3] Thermal tides are planetary-scale gravity waves with periods that are harmonics of the solar day. Tides include westward propagating, migrating (sun-synchronous) waves forced in response to solar heating, and additional nonmigrating waves resulting from zonal variations in the thermotidal forcing. Large amplitude, global-scale variations in martian topography, surface thermal inertia and albedo provide significant forcing for both stationary waves and nonmigrating thermal tides [*Zurek*, 1976; *Wilson and Hamilton*, 1996]. *Wilson* [2000] showed that the longitudinal variability of both midlevel (~25 km) morning and afternoon temperatures derived from MGS Thermal Emission Spectrometer (TES) spectra is dominated by nonmigrating tides in low latitudes (± 30°). Model results indicate that these tides can propagate from the lower atmosphere into the thermosphere [*Forbes and Hagan*, 2000; *Wilson*, 2000]. By contrast, stationary waves are unable to propagate to great heights at tropical and summer hemisphere latitudes. In this study we employ a Mars general circulation model (MGCM) to demonstrate that nonmigrating tides can account for the observed longitudinal structure in MGS thermosphere density data.

2. Nonmigrating Thermal Tides

[4] The longitude-time dependence of stationary waves and thermal tides in a fixed local time reference frame may be represented as:

$$A(\lambda, t_{LT}) \sim \sum A_{s,\sigma} \cos\left[(s-\sigma)\lambda + \sigma t_{LT} + \delta_{s,\sigma}\right] \qquad (1)$$

where s is the zonal wavenumber, λ is east longitude, σ is the temporal harmonic ($\sigma = 1$ for the diurnal tide and $\sigma = 2$ for the semidiurnal tide), t_{LT} is the local solar time, $\delta_{s,\sigma}$ is the phase and λ, δ and t_{LT} are expressed in radians. Tides with $s > 0$ ($s < 0$) propagate westward (eastward) while zonally-symmetric tides have $s = 0$. The migrating tides ($s = \sigma$) have no longitude dependence in the sun-synchronous reference frame. An observed zonal wave m variation may be due to a combination of a stationary wave $A_{m,0}$ and a series of nonmigrating tides with $A_{s,\sigma}$ such that $(s - \sigma) = \pm m$ [*Forbes and Hagan*, 2000; *Wilson*, 2000]. For example, an observed wave 2 variation may be attributed to the presence of diurnal period westward ($A_{3,1}$) and eastward propagating ($A_{-1,1}$) components as well as contributions from higher temporal harmonics ($A_{0,2}$, $A_{4,2}$, $A_{1,3}$, $A_{5,3}$, ...). Similarly, an observed wave 3 variation may be due to contributions from $A_{3,0}$, $A_{0,3}$, $A_{-2,1}$, $A_{4,1}$, $A_{-1,2}$, $A_{5,2}$, ...

[5] Classical tide theory suggests that the most prominent components of the eastward propagating, diurnal period response are the diurnal Kelvin waves (DK1, DK2, corresponding to $s = -1$, -2, ...) which are meridionally broad and symmetric solutions of the Laplace Tidal Equation [*Chapman and Lindzen*, 1970]. DK1 has a vertical structure that closely corresponds to the equivalent barotropic Lamb wave [*Wilson and Hamilton*, 1996; *Forbes and Hagan*, 2000] while DK2 is a vertically propagating mode with a wavelength of roughly 90 km and an amplitude that rapidly increases with height. Nonmigrating semidiurnal tides also have long vertical wavelengths. By contrast, the westward propagating nonmigrating diurnal modes have relatively short (<30 km) vertical wavelengths. Density largely reflects the vertical integration of

0094-8276/02/2001GL013975$05.00

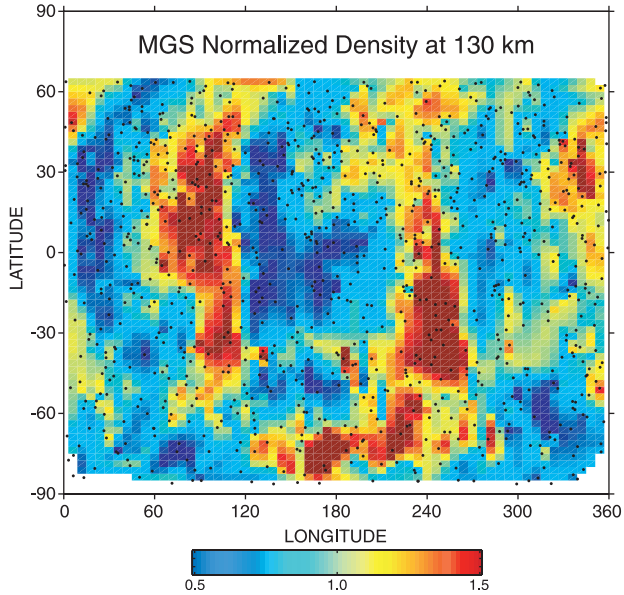

Figure 1. Spatial structure of MGS/ACC density at 130 km normalized by the zonal mean density. Plotted points indicate the distribution of observations which have been interpolated onto a 2.5 by 6 degree latitude-longitude grid. Local solar time advances from 1700 at 60°N to 1400 at 60°S.

temperature so that waves with long vertical wavelengths may efficiently contribute to density variations at thermospheric heights.

3. MGS Density Observations

[6] The MGS Z-axis accelerometer measured the acceleration of the orbiter due to atmospheric drag during the two aerobraking phases of the mission. The analysis of ACC accelerations [*Keating et al.*, 1998; *Tolson et al.*, 2000] has yielded density profiles for altitudes ranging from ~110 to 160 km from both inbound and outbound trajectories. These profiles have been archived on the Planetary Data System [*Keating et al.*, 2001]. Phase 1 aerobraking measurements were obtained from 30° to 50°N for L_s = 183–302°. Phase 2 measurements were obtained during NH spring (L_s = 38–93°), a period when dust storm activity was at a minimum. The smaller orbit and shorter period during Phase 2 allowed the periapsis latitude to precess rapidly southward, providing a broader range of observed latitudes than obtained during Phase 1. Dayside measurements were obtained starting near 60°N at 1700 LT, crossing the equator at 1500 LT and continuing to 60°S at 1400 LT and finally rapidly precessing towards the South Pole. Near the end of Phase 2 aerobraking, nightside (0200 LT) profiles were also obtained for latitudes 30°S to 80°S.

[7] Figure 1 shows the latitude-longitude structure of density at 130 km derived from inbound and outbound trajectories during Phase 2 aerobraking. The density of each observation has been normalized by a fit to the zonal mean density at the corresponding latitude. The time lag between inbound and outbound observations at a given latitude decreased from about 30 days to 10 days as the periapsis latitude migrated southward. There is negligible difference in the meridional variation of zonal mean density derived separately from inbound and outbound observations. There is little difference in the longitude structure of the inbound and outbound density fields, suggesting a fairly steady wave structure.

[8] The zonal wave 2 and wave 3 components of the density field are shown in Figures 2a and 2b, respectively. The wave amplitudes are on the order of 25% and the phases are relatively independent of latitude. Virtually identical patterns are also evident at 140, 150 and 160 km, but with amplitude decaying with altitude. A similar analysis (not shown) performed on nightside density variations indicates a complete reversal in phase between the day (1400 LT) and night (0200 LT) zonal wave 2 fields, suggesting a diurnal tide. By contrast, there is only a modest shift in phase between the day and nightside wave 3 fields which would be consistent with a semidiurnal tide.

4. MGCM Tide Simulation

[9] We now turn to an examination of zonal density variations in an MGCM simulation of the NH spring season. The Geophysical Fluid Dynamics Laboratory MGCM is described in *Wilson and Hamilton* [1996]. Here we use a version of the model with 50 levels extending to 9×10^{-8} mb (~130 km). The MGCM does not yet incorporate realistic descriptions of the dissipative and thermal damping processes (particularly non-LTE effects on IR cooling by CO_2) that become increasingly important above 70 km. We have therefore employed a Newtonian cooling parameterization to approximate the radiative transfer in this region of the atmosphere. This limitation does compromise the simulation of the component of the migrating thermal tide which is strongly forced by in-situ solar heating in the upper atmosphere. However, our specification of thermal damping has significantly less effect on the nonmigrating tides investigated here, which are forced by zonal variations in thermotidal forcing in the lower atmosphere.

[10] The simulation employs a relatively small dust column opacity (~0.4) and, as in *Wilson* [2000], yields temperatures and nonmigrating tide fields that are consistent with MGS TES temperatures at 25 km for this season. Figures 2c and 2d shows the wave 2 and 3 components of the simulated dayside (1400 LT) density at 120 km for L_s = 80°. A comparison with Figures 2a and 2b indicates that the simulated amplitude and phase are in reasonable agreement with the observed fields.

[11] The simulated density field may be readily decomposed into stationary wave ($A_{s,0}$) and eastward and westward propagating tide ($A_{s,\sigma}$) components. Figure 3 shows the latitude-height structure of normalized density for the principal modes responsible for the wave fields in Figures 2c and 2d. The dominant contribution to the

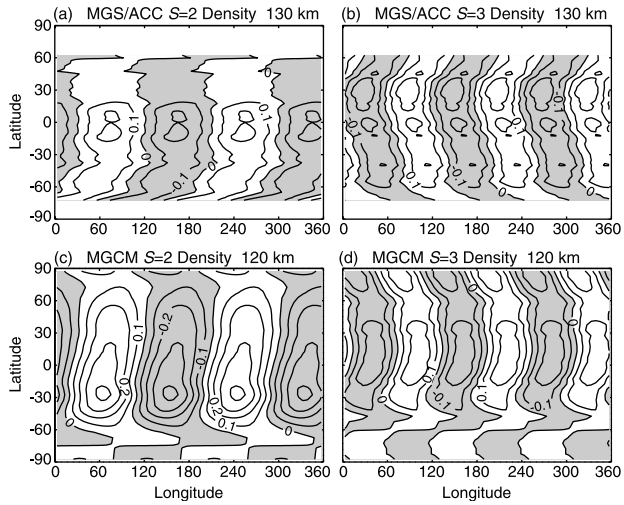

Figure 2. Comparison of the spatial structures of the zonal wave 2 (left) and wave 3 (right) components of the MGS/ACC density field shown in Figure 1 (top panels) and the corresponding fields from the MGCM simulation (bottom panels). The simulated fields correspond to 1400 LT at L_s = 80°. The contour interval is 0.1 and shading indicates negative deviations from the zonal mean.

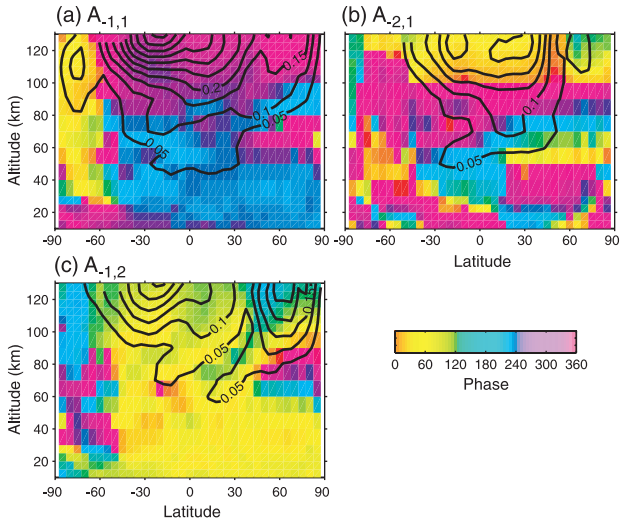

Figure 3. Latitude-height variation of amplitude and phase of the simulated (a) eastward propagating, diurnal period zonal wave 1 ($A_{-1,1}$), (b) eastward propagating, diurnal period zonal wave 2 ($A_{-2,1}$), and (c) eastward propagating, semidiurnal period, zonal wave 1 ($A_{-1,2}$). Amplitudes are contoured at intervals of 0.05 and the phase is indicated by color shading.

simulated zonal wave 2 pattern is due to the diurnal period, eastward propagating wave ($A_{-1,1}$) shown in Figure 3a. The meridional and vertical structure is consistent with that of DK1 [*Forbes and Hagan*, 2000; *Wilson*, 2000]. The phase reversal exhibited by the day and night wave 2 ACC density fields supports this diurnal wave interpretation.

[12] The principal components of the simulated zonal wave 3 field are eastward propagating, diurnal wave 2 ($A_{-2,1}$) and eastward propagating, semidiurnal wave 1 ($A_{-1,2}$) shown in Figures 3b and 3c, respectively. The $A_{-2,1}$ component has the meridional and vertical structure of DK2 [*Wilson*, 2000] while $A_{-1,2}$ has a very long vertical wavelength consistent with classical tidal theory calculations. Plots of the longitude-height structure of equatorial wave 2 and 3 density (not shown) correlate closely with the corresponding geopotential sections in Figure 5 of *Wilson* [2000] and clearly indicate the barotropic character of $A_{-1,1}$.

5. Discussion and Conclusions

[13] We now consider additional data and model results that support the simulation results presented in the preceding section. An examination of the atmospheric response to the selective removal of zonal wave harmonics of topography, surface thermal inertia and albedo confirms that the simulated nonmigrating tides are forced by zonal wave 1 – 3 components in the surface boundary conditions. In particular, it is readily shown that DK1 is forced by the zonal wave 2 component of topography [*Wilson and Hamilton*, 1996].

[14] The meridional structure and phase of the observed and simulated wave 2 density variations at 130 km (Figure 2) are in close agreement with the observed wave 2 structure in TES temperatures at 25 km collected during the MGS mapping mission [*Wilson*, 2000]. The phase of the simulated wave 2 density variation also matches the phase of the DK1 inferred from surface pressure observations at the two Viking lander sites [*Wilson and Hamilton*, 1996]. This agreement in phase for observed zonal wave 2 fields at the surface, 25 km and 130 km is consistent with the barotropic vertical structure that is characteristic of DK1. The phases of tropical wave 2 and 3 temperature structures in the TES data show little change with season which suggests that the wave 2 density variation observed during Phase 1 [*Keating et al.*, 1998] is also attributable to DK1 [*Forbes and Hagan*, 2000].

[15] The MGCM results indicate that $A_{-1,2}$ and $A_{-2,1}$ are the dominant contributors to the observed wave 3 density field. We have verified that the structure of these nonmigrating tide components is robust by varying our description of solar heating and Newtonian damping in the upper atmosphere. It should be noted however, that the relative strength of these two modes may be sensitive to the formulation of radiative damping in the upper atmosphere. In particular, unlike Newtonian damping, realistic radiative damping is scale selective, so that the shorter vertical wavelength of $A_{-2,1}$ relative to $A_{-1,2}$ could result in preferential attenuation of the diurnal component at thermosphere altitudes. For example, Figures 3b and 3c indicate that the amplitude of $A_{-1,2}$ is comparable to that of $A_{-2,1}$ in the 30–60°S latitude range, while the modest phase shift between wave 3 night and day ACC density fields suggests that the semidiurnal tide is dominant at these latitudes.

[16] The presence of DK2 in the tropics provides a consistent simulation of the observed wave 3 amplitude and structure in TES tropical temperatures at 25 km [*Wilson*, 2000] and density at 130 km. An examination of TES limb temperature retrievals indicates that DK2 is prominent in the tropics up to at least 60 km in altitude.

[17] Figure 3c shows a prominent semidiurnal tide response at high northern latitudes which is consistent with a recent analysis of MGS Radio Science electron density profiles at 66–67°N that indicates a wave 3 density variation at 0400 LT that is in phase with the ACC density variation observed at 1700 LT [*Bougher et al.*, 2001]. The amplitude (~2 km at 110 km) and phase of the simulated wave 3 geopotential variation at 0400 LT (not shown) are in good agreement with the observations, and the simulation captures the 30° eastward shift in phase between 110 and 135 km shown in Fig. 2 in *Bougher et al.* [2001].

[18] In summary, we find that eastward propagating, nonmigrating tides can account for much of the planetary scale wave structure observed in MGS accelerometer density data (in a fixed local time reference). These waves result from topographic modulation of the thermotidal response to migrating solar insolation. The wave 1 diurnal Kelvin mode provides a consistent description of the observed wave 2 structure in density at 130 km, TES temperatures at 25 km [*Wilson*, 2000] and Viking surface pressure data [*Wilson and Hamilton*, 1996]. The observed wave 3 density variation is largely due to a wave 2 diurnal Kelvin mode and an eastward-propagating wave 1 semidiurnal tide. The continued investigation of these waves will be important for understanding the structure and variability of the martian atmosphere at aerobraking altitudes.

[19] **Acknowledgments.** The author would like to thank Paul Withers, Steve Bougher, Dave Hinson, and Jeff Forbes for helpful comments. This work was supported by a grant from the NASA Mars Data Analysis program. The ACC dataset [*Keating et al.*, 2001] is available at the Planetary Atmospheres Node of the Planetary Data System: http://atmos.nmsu.edu.

References

Bougher, S. W., S. Engel, D. P. Hinson, and J. M. Forbes, Mars Global Surveyor Radio Science electron density profiles: Neutral atmosphere implications, *Geophys. Res. Lett.*, *28*, 3091–3094, 2001.

Chapman, S., and R. S. Lindzen, *Atmospheric Tides*, 201 pp., D. Reidel, Norwell, MA, 1970.

Forbes, J. M., and M. E. Hagan, Diurnal Kelvin wave in the atmosphere of Mars: Towards an understanding of 'stationary' density structures observed by the MGS Accelerometer, *Geophys. Res. Lett.*, *27*, 3563–3566, 2000.

Joshi, M. M., J. L. Hollingsworth, R. M. Haberle, and A. F. C. Bridger, An interpretation of Martian thermospheric waves based on analysis of a general circulation model, *Geophys. Res. Lett.*, *27*, 613–616, 2000.

Keating, G. M., et al., The structure of the upper atmosphere of Mars: In situ accelerometer measurements from Mars Global Surveyor, *Science*, *279*, 1672–1676, 1998.

Keating, G. M., R. H. Tolson, J. L. Hanna, R. F. Beebe, J. R. Murphy, and L. F. Huber, MGS-M-ACCEL-5-ALTITUDE-V1.0, *NASA Planetary Data System*, 2001.

Tolson, R. H., G. M. Keating, S. N. Noll, D. T. Baird, and T. J. Shellenberg, Utilization of Mars Global Surveyor Accelerometer data for atmospheric modeling, *Adv. Astronautical Sci.*, *103*, 1329–1346, 2000.

Wilson, R. J., Evidence for diurnal period Kelvin waves in the martian atmosphere from Mars Global Surveyor TES data, *Geophys. Res. Lett.*, *27*, 3889–3892, 2000.

Wilson, R. J., and K. Hamilton, Comprehensive Model Simulation of Thermal Tides in the Martian Atmosphere, *J. Atmos. Sci.*, *53*, 1290–1326, 1996.

Withers, P., S. W. Bougher, and G. M. Keating, New Results from Mars Global Surveyor Accelerometer, *31st Lunar and Planetary Science Conference*, Abstract #1268. LPI Contribution No. 1000, Lunar and Planetary Institute, Houston (CD-ROM), 2000.

Zurek, R. W., Diurnal tide in the martian atmosphere, *J. Atmos. Sci.*, *33*, 321–337, 1976.

R. J. Wilson, GFDL/NOAA, P.O. Box 308, Princeton, NJ 08542, USA. (rjw@gfdl.noaa.gov)